Spectral simulation of GaAs and InAs quantum-dot terahertz detectors designed for higher-temperature operation

I. Vurgaftman, J. R. Meyer, D. H. Wu, K. Bussmann, and B. T. Jonker

Citation: J. Appl. Phys. **100**, 064509 (2006); doi: 10.1063/1.2349556
View online: http://dx.doi.org/10.1063/1.2349556
View Table of Contents: http://jap.aip.org/resource/1/JAPIAU/v100/i6
Published by the American Institute of Physics.

Spectral simulation of GaAs and InAs quantum-dot terahertz detectors designed for higher-temperature operation

I. Vurgaftman,[a] J. R. Meyer, D. H. Wu, K. Bussmann, and B. T. Jonker
Code 5613, Naval Research Laboratory, Washington D.C. 20375

(Received 16 May 2006; accepted 5 July 2006; published online 26 September 2006)

The spectral properties and other performance characteristics of single-photon quantum-dot terahertz detectors incorporating single-electron transistors are analyzed for the cases of GaAs and InAs electron channels. By defining the electrostatically confined double-quantum-dot structures in shallow two-dimensional electron gas structures, these devices have the potential to operate at temperatures above the dilution refrigerator range. We calculate the interlevel plasmon absorption by using the random-phase approximation in conjunction with realistic band structures and three-dimensional confinement geometries. While the level separations increase with decreasing dot diameter, carrier depletion eventually limits the minimum size that is viable. The maximum detection frequency is about 1 THz for GaAs channels, but increases to 1.5–2 THz for InAs channels having a lower effective mass.
[DOI: 10.1063/1.2349556]

INTRODUCTION

While single-photon detectors are now readily available for the near-infrared and visible wavelengths, there is no commercially available single-photon detector for frequencies below mid-infrared; the sensitivities of longer-wavelength commercial photodetectors are poorer by many orders of magnitude. The terahertz spectral region, which is loosely defined to be from 0.1 to 10 THz, is especially challenging and also important since much interesting spectroscopy and imaging can be obtained in that region. Remarkable progress was made recently[1–3] when a quantum-dot absorber, formed by the electrostatic depletion of a high-mobility two-dimensional electron gas (2DEG), was coupled to a quantum-dot single-electron transistor[4,5] (SET). This work culminated in the demonstration of single-photon detection at 0.5 THz.[6] However, the operating temperature did not exceed 100 mK. These devices would have a much more practical value if a dilution refrigerator were not required. It would also be beneficial to extend the detectable wavelength range, with higher frequencies being of particular concern for spectroscopy.

In this paper, we address these issues by carrying out a detailed theoretical analysis of the subband structure and terahertz absorption spectra as a function of quantum-dot size, and for realistic three-dimensional (3D) geometries based on both GaAs and InAs 2DEGs. In the double-dot approach,[6] the SET resonance voltages associated with the first dot are sensitive to the number of electrons in the second dot, which functions as a photon absorber and is coupled to an antenna. While the absorption occurs via a plasmon excitation process, relaxation of the plasmon system eventually results in the expulsion of an electron from the second dot. This shifts the Fermi level in the SET by e^2C_{12}/C_1C_2, where C_1 and C_2 are the total capacitances of the two dots and C_{12} is the interdot capacitance. Typically, C_{12} is designed to be roughly an order of magnitude smaller than C_1 and C_2. With proper adjustment of the SET plunger gate voltage in the dark, this capacitive coupling can induce the shift to a conductance peak under illumination, leading to the capability of single-photon detection. Our assumed geometry will be similar to that of the prototypical structure of Ref. 6, in which both dots are formed in a buried modulation-doped 2DEG layer by applying a reverse bias to patterned surface electrodes. The higher potential under the metal gates depletes carriers from those regions.

PRACTICAL CONSIDERATIONS

Since the terahertz detectors demonstrated thus far have employed relatively deep 2DEGs ($d \approx 100$ nm) and relatively large-diameter quantum dots ($D \geqslant 500$ nm),[3,6] their operation required a dilution refrigerator. This temperature limitation was dictated mostly by the properties of the SET rather than those of the terahertz absorber. It may be possible to raise the temperature, as pronounced single-electron charging effects have been observed up to 4 K in a shallower 2DEG ($d \approx 30$ nm) with $D=150$ nm.[7] The smaller dot reduces the capacitance (a useful approximate relationship is $C \approx 4\varepsilon D$), while the shallower 2DEG minimizes "smearing" of the effective potential at a depth d when a bias is applied to the surface contacts. In fact, the smallest dot size that is practical for a given 2DEG depth follows an approximate empirical relation $D \geqslant 5d$. Any further decrease of D fully depletes the dot's electron population, making the dot nonfunctional either as a absorber or as a SET island. It appears that a high sensitivity (if not single photon) detection should become possible at 4 K if a shallow 2DEG is employed to form the double-dot detector.

We should consider a possible degradation of the device functionality as a consequence of the shallow 2DEG's lower mobility (μ), which is caused by the greater wave function overlap with the donor and surface layers. Note first that a

[a]Electronic mail: vurgaftman@nrl.navy.mil

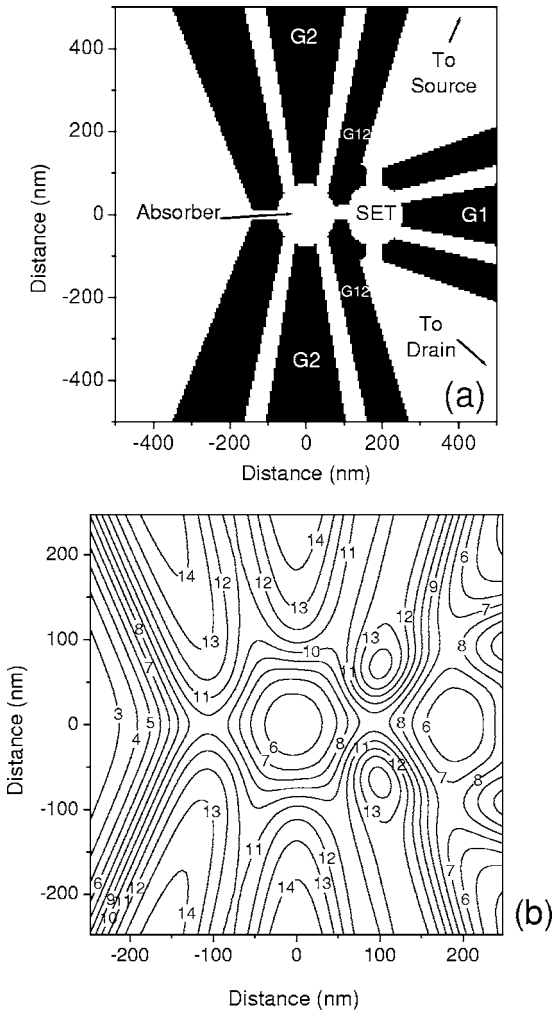

FIG. 1. (a) Schematic drawing and (b) a contour plot of the in-plane potential for the double-dot terahertz detector using a GaAs 2DEG. The potential contours are spaced by 1 meV.

high sensitivity quantum-dot detector has been demonstrated using a 2DEG with $\mu = 8 \times 10^5$ cm^2/V s,[3] which is only slightly higher than the mobility of 3×10^5 cm^2/V s reported for the 30-nm-deep 2DEG.[7,8] This value does not represent the upper bound, since the growth quality and structural details tend to vary, and $\mu > 10^6$ cm^2/V s has been reported for other shallow 2DEGs.[9] The SET operation does *not* require $\mu \geqslant 10^6$ cm^2/V s,[7] and the enhanced boundary scattering induces only a modest additional broadening of the absorption spectrum ($\approx$0.2 meV for $\mu = 3 \times 10^5$ cm^2/V s). While the shallow 2DEG's lower mobility may affect the noise-equivalent power due to an increased dark-switching rate,[6] we do not expect the impact to be significant. In general, the dark-switching rate and saturation power, which is inversely proportional to the lifetime of the ionized state, are quantities of interest. However, both are quite difficult to calculate, and they are beyond the scope of this paper.

Figure 1(a) schematically illustrates a typical two-dot design with $D = 150$ nm. While both dots are taken to have the same size for convenience (here and in the other examples below), often one needs to employ different-size dots to achieve a more desirable result. While the SET dot should generally be as small as possible, provided that the size is

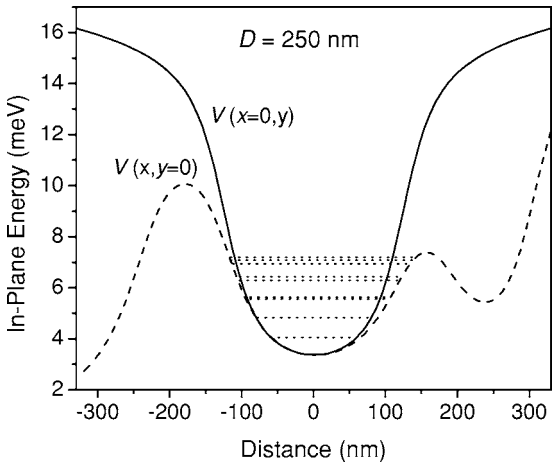

FIG. 2. In-plane potential profiles along the x axis and y axis, shown with selected subband energy levels, for the structure in Fig. 1 with the dot diameter of 250 nm for both dots.

within the limit satisfying the potential resolution achievable for a given 2DEG depth, it will be seen below that varying the absorber dot diameter provides a means for tuning the terahertz spectral properties. We assume a shallow 2DEG ($d = 30$ nm) similar to that of Ref. 7, with a 25-nm-thick layer of $Al_{0.3}Ga_{0.7}As$ grown on top of the thick GaAs channel. The delta doping in the middle of the $Al_{0.3}Ga_{0.7}As$ layer is surrounded on both sides by 1 ML (monolayer) of GaAs, and a 5-nm-thick GaAs cap completes the structure. The vertical band diagram is quite similar to examples that have appeared previously.[10] The dark regions of Fig. 1(a) represent the deposited metallic electrodes, whereas the light surface areas are bare. The plunger gates for the SET dot on the right (G_1) and the absorber dot on the left (G_2) are specified, while the capacitive coupling between the two dots is controlled by the contacts marked G_{12}. The assumed 2DEG density of $n_{2D} = 5 \times 10^{11}$ cm^{-2} requires $\sim 4 \times 10^{12}$ cm^{-2} Si atoms[11] in the delta-doping layer.

GAAS-BASED DEVICES

The 3D spatial profiles of the carrier density and electrostatic potential were calculated for the structure shown in Fig. 1(a) by solving Poisson's equation self-consistently. Figure 1(b) shows a contour plot of the resulting in-plane electrostatic potential at the 2DEG depth (excluding the vertical quantization energy in the triangular potential well, which is proportional to[10] $n_{2D}{}^{2/3}$). For GaAs near the conduction-band minimum, the simulation employed a parabolic approximation with an effective mass of $0.067m_0$. For a structure similar to that of Fig. 1 but with $D = 250$ nm, Fig. 2 illustrates the in-plane potential profiles along the x and y axes, along with selected energy levels for states localized in the absorbing dot. The depth of the potential well with respect to the top of the lowest barrier is $\sim$4 meV.

Next, the 2D potential of Fig. 1(b) is used to compute the absorption spectrum of the left dot. Spin-degenerate energy levels and wave functions of the absorbing states are calculated using a finite-difference approximation to Schrödinger's equation. For simplicity, low-potential regions far away from the dot are not included in the simulation,

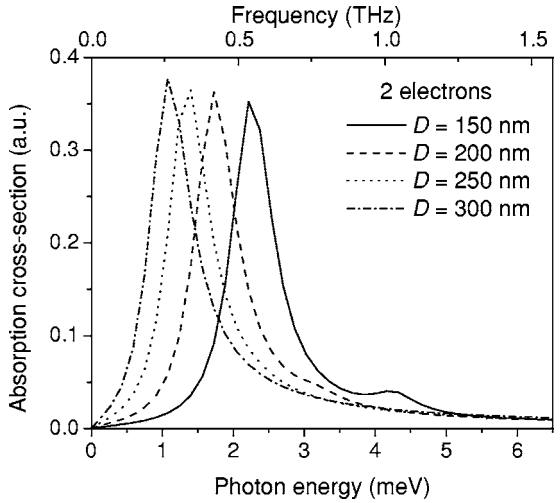

FIG. 3. Absorption cross section for the $D=150$ nm (solid), 200 nm (dash), 250 nm (dot), and 300 nm (dash-dot) quantum dots containing two electrons (GaAs 2DEG).

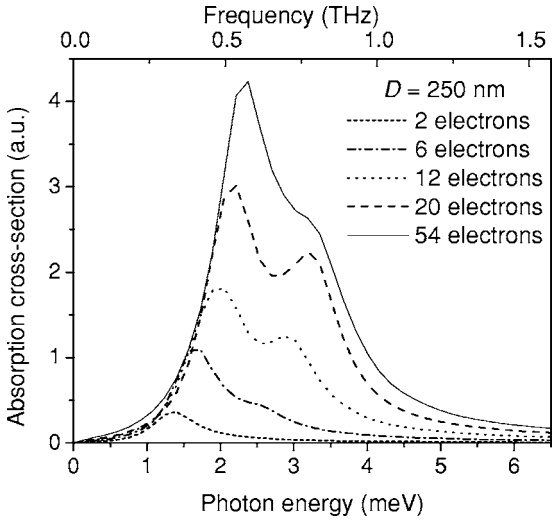

FIG. 4. Absorption cross section for the $D=250$ nm quantum dot with 2, 6, 12, 20, and 54 electrons (GaAs 2DEG).

along with absorption in those regions. Within the random-phase approximation (RPA), the charge density induced by the external electromagnetic radiation V^{em} with frequency ω is given by[12,13]

$$\delta\rho(\mathbf{r}) = \int d\mathbf{r}' \sum_n \sum_{n'} \frac{f_n - f_{n'}}{\varepsilon_n - \varepsilon_{n'} + \hbar\omega + i\gamma} \times \psi_n(\mathbf{r})\psi_n(\mathbf{r}')\psi_{n'}(\mathbf{r})\psi_{n'}(\mathbf{r}') \times \left[V^{\mathrm{em}}(\mathbf{r}') + \int d\mathbf{r}'' \frac{e^2\delta\rho(\mathbf{r}'')}{4\pi\varepsilon|\mathbf{r}' - \mathbf{r}''|} \right]. \quad (1)$$

Here the summation is over the quantum-dot states n and n', which have occupations f, energies ε, and wave functions ψ. The assumed linewidth of $\gamma=0.35$ meV, which is consistent with the broadening observed in Ref. 6 and also with the mobility measured in Ref. 7, is attributable in part to the decay of plasmons into single-particle excitations. The second term in square brackets accounts for the many-particle nature of the absorption and makes Eq. (1) an integral equation. For a terahertz radiation beam polarized along an in-plane axis (say, x): $V^{\mathrm{em}}=E^{\mathrm{em}}x$, and the absorption cross section is given by $\sigma(\omega)=4\pi(\varpi/c)\mathrm{Im}[(1/E^{\mathrm{em}})\int d\mathbf{r}x\delta\rho(\mathbf{r})]$. We solve Eq. (1) numerically on a finite mesh in the $\mathbf{r}$ plane by casting it as the following matrix equation:

$$P = XV + XEP, \quad (2)$$

where P is a charge density vector with entries corresponding to each discrete point in the $\mathbf{r}$ plane, X is the susceptibility matrix in $\mathbf{r}$ and $\mathbf{r}'$ corresponding to the term under the summations in Eq. (1), and E is the Coulomb matrix $e^2/(4\pi\varepsilon|\mathbf{r}-\mathbf{r}'|)$. Equation (2) is readily manipulated to yield

$$P = \frac{XV}{I - XE}, \quad (3)$$

where I is the identity matrix.

The position of the plasmon absorption peak depends on both the size of the quantum dot and the number of electrons in the dot. To illustrate the former point, Fig. 3 plots the absorption spectra for dots with diameters of 150, 200, 250, and 300 nm, where each dot is assumed to contain only two electrons (one fully occupied spin-degenerate level). The absorption peak's steady blueshift mirrors an increase in the separation between energy levels at the Fermi level (from 0.5 meV for the 350 nm dot to 1.4 meV for the 150 nm dot). We emphasize, however, that the peak energy is noticeably larger than the level spacing, a many-body effect[12] associated with the second term in brackets in Eq. (1).

Both the position and the amplitude of the absorption peak depend on the number of electrons in the dot. The absorption spectra in Fig. 4, corresponding to $D=250$ nm, illustrate that as the number of electrons increases from 2 to 54 electrons, there is a blueshift accompanied by pronounced broadening and the appearance of a shoulder peak. Near the bottom of the dot, the potential is very nearly parabolic and circularly symmetric [see Fig. 1(b)]. Thus with few electrons and a low Fermi energy, the potential is harmonic and the spacing of the energy levels is nearly constant (with the degeneracy increasing by two, including spin, for each successive level). However, as the number of electrons increases (or the dot size decreases), the Fermi level moves into the nonharmonic potential region where higher-order transitions become allowed. We estimate that without any artificial adjustment of the Fermi level, the dot with $D=250$ nm should contain 54 electrons, which is considerably less than the geometrical value of $n_{2\mathrm{D}}(\pi/4)D^2$. This is due in part to potential smearing in the nearby contacts. The calculation also confirms that a dot size appreciably smaller than 150 nm is impractical, since the dot is then completely depleted.

From the absorption spectra for a series of dot sizes (150–350 nm) in Fig. 5, we find that even the shallow 2DEGs assumed in this paper do not benefit from a dot diameter smaller than ~250 nm. Smaller dots fail to induce any further extension of the spectral range because the redshift associated with reduced electron population balances the blueshift due to stronger quantum confinement. On the other hand, the absorption in dots larger than 250 nm is weakened by Pauli blocking effects that prevent electrons

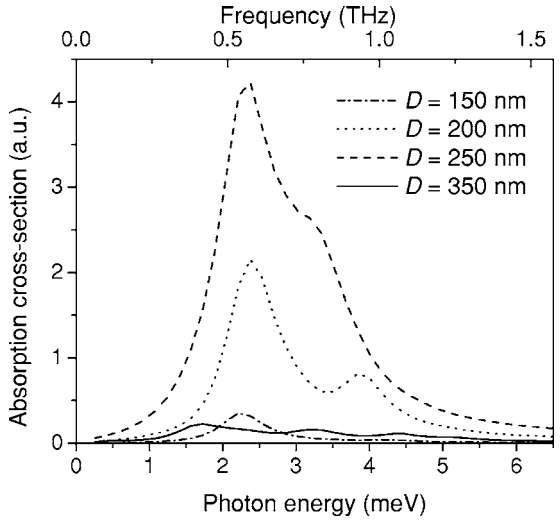

FIG. 5. Absorption cross section for the $D=150$ nm (dash-dot), 200 nm (dot), 250 nm (dash), and 350 nm (solid) quantum dots with a realistic number of electrons (GaAs 2DEG).

near the bottom of the well from participating in the optical transitions. The figure shows that relatively strong absorption is obtained to frequencies of 0.8–1.5 THz. Note, however, that the absorption spectra in this paper do not account for the antenna coupling (without which the absorption would be negligible) or its wavelength dependence.

NARROW-GAP DEVICES

Although all of the quantum-dot terahertz detector structures demonstrated to date have employed GaAs-based 2DEGs, we next consider whether the frequency range can be extended beyond 1 THz by adopting a material with a smaller effective mass and hence larger interlevel spacing. An obvious candidate is the InAs 2DEG system, since its band-edge mass is a factor of 2.5 smaller than that of GaAs.[14] Another attractive feature is that mobilities approaching 10^6 cm^2/V s have been demonstrated.[15] We simulate a structure whose 20 nm InAs quantum well (QW) is sandwiched by $Al_{0.8}Ga_{0.2}Sb$ barriers, as shown in the band diagram of Fig. 6(a). The structure is quite similar to that in Ref. 15, except that the 25-nm-thick top barrier is capped by a much thinner GaSb layer (5 nm instead of 30 nm) to place the 2DEG at approximately the same depth as the shallow GaAs 2DEG considered above. A single delta-doping layer, positioned 10 nm above the QW interface, is taken to induce a total two-dimensional (2D) carrier density of 6×10^{11} cm^{-2}. The lattice constant is assumed to be that of the thick $Al_{0.8}Ga_{0.2}Sb$ buffer layer, since the QW width is less than the critical thickness. Because our primary interest is in exploring potential advantages of the alternative InAs 2DEG material system, we assume sufficiently high fabrication quality for proper functioning of the SET and terahertz detector, even though the present structure may have a somewhat lower mobility than that reported in Ref. 15.

Since the single-band approximation employed above becomes invalid for narrow-gap devices, we follow an alternative strategy that similarly limits the computational time. First, the band structure along the vertical axis is derived

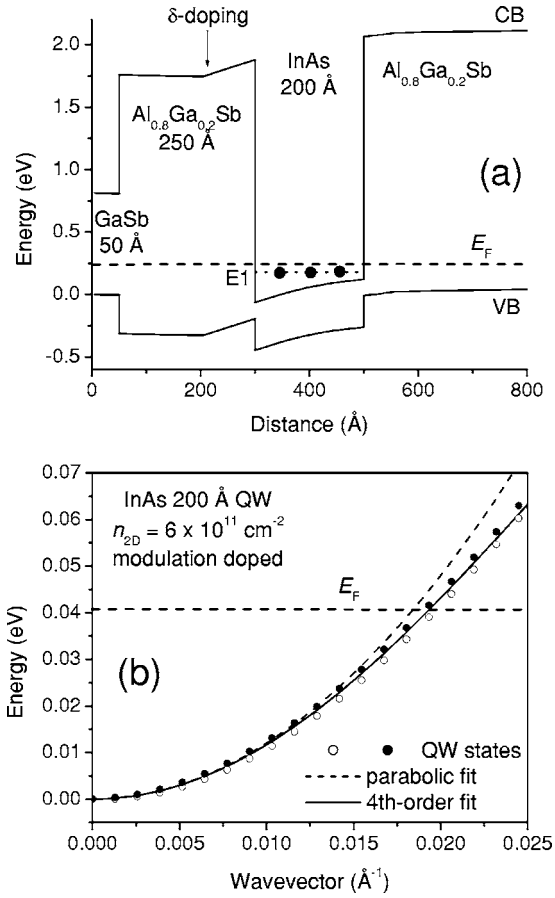

FIG. 6. (a) Vertical band diagram of an InAs 2DEG and (b) a fitted dispersion for the lowest conduction subband of the InAs quantum well.

from the standard eight-band $\mathbf{k}\cdot\mathbf{p}$ theory. The resulting in-plane dispersion for the lowest subband of the InAs QW is next fitted to the simple nonparabolic form $E(k)=(\hbar^2k^2/2m^*)-\alpha k^4$. The points in Fig. 6(b) plot the dispersion relations calculated from the eight-band $\mathbf{k}\cdot\mathbf{p}$ model, while the solid curve represents the fit. For simplicity we neglect the Rashba splitting and in-plane anisotropy, which are quite small in the present structure. The fit, based on the parameters $m^*=0.0318m_0$ and $\alpha=3.0\times10^4$ Å^4, is seen to accurately reproduce the eight-band result, whereas the parabolic approximation (dashed curve) breaks down at energies near the Fermi level.

To calculate the spin-degenerate quantum-dot states and the self-consistent in-plane electrostatic potential, the fitted dispersion relation is employed with the standard substitution $k\rightarrow-i\nabla$. The discrete form of the Schrödinger-like equation is then

$$\frac{\hbar^2}{2m^*}\frac{-\psi_{i+1}+2\psi_i-\psi_{i-1}}{(\Delta x)^2}-\alpha\frac{\psi_{i+2}-4\psi_{i+1}+6\psi_i-4\psi_{i-1}+\psi_{i-2}}{(\Delta x)^4}+V\psi_i=E\psi_i. \tag{4}$$

While for simplicity we indicate only one spatial dimension with constant mesh pitch Δx, the generalization to a second Cartesian dimension is straightforward.

We again assume a double-quantum-dot structure similar to that depicted in Fig. 1, except that the effective in-plane potential barrier is now larger by more than a factor of 2 due

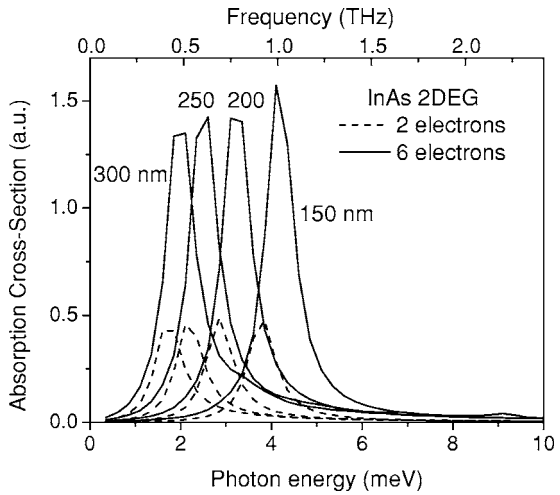

FIG. 7. Absorption cross section for the $D=150$, 200, 250, and 350 nm quantum dots with two (dashed) and six (solid) electrons (InAs 2DEG).

to the smaller mass. Figure 7 plots the absorption spectra calculated for several InAs-based dots with sizes $D=150$, 200, 250, and 300 nm, and with both two (dashed) and six (solid) electrons. Comparison with Figs. 3 and 4 indicates a shift to shorter wavelengths of the resonance peaks for dots with the same size and number of electrons. This is an expected consequence of the larger (by about a factor of 2 compared to GaAs-based) interlevel spacings resulting from the smaller effective mass, e.g., 0.86 meV for the 400 nm dot, 1.67 meV for the 250 nm dot, and 2.95 meV for the 150 nm dot.

Absorption spectra for InAs-based dots with several sizes and realistic carrier occupation numbers are shown in Fig. 8. Note that the high-frequency shoulder features are less pronounced here than in Figs. 4 and 5. Partial depletion substantially reduces the absorption magnitude when $D=150$ nm, and the depletion becomes complete at diameters approaching 100 nm. Thus the smallest practical size for an InAs-based dot is ~200 nm. We find that significant absorption may be attainable up to 1.5–2 THz, which should be compared to ~1 THz for the GaAs-based structures considered above and ~0.6 THz for the demonstrated detectors with relatively deep (~100 nm) GaAs 2DEGs.[3,6]

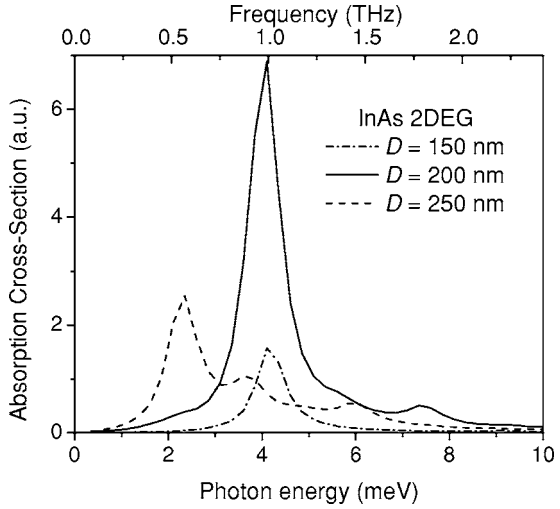

FIG. 8. Absorption cross sections for InAs-based dots with diameters of 150 nm (dash-dot), 200 nm (solid), and 250 nm (dashed) and realistic electron populations (2, 16, and 58 electrons, respectively).

DISCUSSION

Finally, we briefly consider the maximum operating temperature of the quantum-dot terahertz photodetector. For the device to function as a photon counter, each absorption process must remove at least one electron from the absorbing dot. Physically, this occurs when the plasmon excitation decays into a single-particle excitation on a time scale of a few picoseconds,[6] and the decay of plasmon excitation gives the excited electron enough energy to escape the dot via one of the barriers. While the expulsion can, in principle, occur by tunneling, the electron's energy must be close enough to the top of the barrier that the escape lifetime is shorter than the energy relaxation time within the dot. This means that the top of the lowest barrier must be close to $\sim\hbar\omega$ above the Fermi level (the latter being fine tuned by the bias on the G_2 plunger gate) Furthermore, to maintain an acceptably low dark-switching rate, the maximum operating temperature $T_{\max}$ should be kept low to satisfy the condition $k_B T_{\max} \ll \hbar\omega$. For the devices discussed in this paper, this implies $T_{\max} \leqslant 5-10$ K. This additional requirement to operate the SET at $T_{\max}$ imposes an upper limit on the diameter of the SET dot, as was discussed in the Introduction.

In summary, we have designed high-sensitivity double-dot terahertz detectors based on shallow GaAs and InAs 2DEGs, and calculated their absorption characteristics. Because the dots can be made smaller and the subband separations thereby increased, these structures promise to allow the single-electron transistor operation at or above the liquid-helium temperature. We predict a high photon absorption rate at frequencies of up to 1 THz for the quantum-dot detector made of GaAs and 1.5–2 THz for the InAs devices. The SET dot can be very small as long as complete electron depletion is avoided. The minimum size of the photon absorber dot is also limited by a spectral redshift in a smaller dot with a reduced number of carriers.

ACKNOWLEDGMENTS

This work was supported by ONR and the Nano Science Institute at the Naval Research Laboratory.

[1] S. Komiyama, O. Astafiev, V. Antonov, T. Kutsuwa, and H. Hirai, Nature (London) **403**, 405 (2000).
[2] O. Astafiev, V. Antonov, T. Kutsuwa, and S. Komiyama, Phys. Rev. B **62**, 16731 (2000).
[3] O. Astafiev, S. Komiyama, and T. Kutsuwa, Appl. Phys. Lett. **79**, 1199 (2001).
[4] U. Meirav and E. B. Foxman, Semicond. Sci. Technol. **11**, 255 (1996).
[5] K. K. Likharev, Proc. IEEE **87**, 606 (1999).
[6] O. Astafiev, S. Komiyama, T. Kutsuwa, V. Antonov, Y. Kawaguchi, and K. Hirakawa, Appl. Phys. Lett. **80**, 4250 (2002).
[7] Z. Borsosfoldi, M. Rahman, I. A. Larkin, A. R. Long, J. H. Davies, J. M. R. Weaver, M. C. Holland, and J. G. Williamson, Appl. Phys. Lett. **66**, 3666 (1995).
[8] M. C. Holland, E. Skuras, J. H. Davies, I. A. Larkin, A. R. Long, and C. R. Stanley, J. Cryst. Growth **150**, 1215 (1995).
[9] J. E. F. Frost, D. A. Ritchie, and G. A. C. Jones, J. Cryst. Growth **111**, 305 (1991).

[10]A. R. Long, J. H. Davies, M. Kinsler, S. Vallis, and M. C. Holland, Semicond. Sci. Technol. **8**, 1581 (1993).
[11]E. Skuras, M. C. Holland, C. J. Barton, J. H. Davies, and A. R. Long, Semicond. Sci. Technol. **10**, 922 (1995).
[12]D. A. Broido, K. Kempa, and P. Bakshi, Phys. Rev. B **42**, 11400 (1990).
[13]V. Gudmundsson and R. R. Gerhardts, Phys. Rev. B **43**, 12098 (1991).
[14]I. Vurgaftman, J. R. Meyer, and L. R. Ram-Mohan, J. Appl. Phys. **89**, 5815 (2001).
[15]H.-R. Blank, M. Thomas, K. C. Wong, and H. Kroemer, Appl. Phys. Lett. **69**, 2080 (1996).